ORIGINAL PAPER

Effects of cellulose nanofibrils on the structure and properties on PVA nanocomposites

Dagang Liu · Xun Sun · Huafeng Tian · Sonakshi Maiti · Zhongshi Ma

Abstract A green method—joint mechanical grinding and high pressure homogenization—was used to defibrillate paper pulp into nanofibrils. The prepared cellulose nanofibrils (CNF) were then blended with PVA in an aqueous system to prepare transparent composite film. The size and morphology of the nanofibrils and their composites were observed, and the structure and properties were characterized. The results showed that CNFs are beneficial to improve the crystallinity, mechanical strength, Young's modulus, T_g and thermal stability of the PVA matrix because of their high aspect ratio, crystallinity and good compatibility. Therefore, nano cellulosic fibrils were proven to be an effective reinforcing filler for the hydrophilic polymer matrix. Moreover, the green fabrication approaches will be helpful to build up biodegradable nanocomposites with wide applications in functional environmentally friendly materials.

D. Liu (✉) · X. Sun · S. Maiti · Z. Ma
Department of Chemistry, Nanjing University
of Information Science and Technology,
Nanjing 210044, China
e-mail: dagang@nuist.edu.cn; dangliu@gmail.com

H. Tian
Department of Materials Science and Engineering,
Beijing Technology and Business University,
Beijing 100048, China

Introduction

Nanocomposites are a new class of composites with at least one phase having at least one dimension in the vicinity of 1–100 nm. Nowadays, inorganic nanofillers are mostly used to prepare nanocomposites with polymeric matrices (Schmidt and Malwitz 2003), although their processability, biocompatibility and biodegradability are much more limited than those of naturally organic ones. In nature, a large number of living beings can produce extracellular high-performance structural biocomposites that consist of a matrix reinforced with fibrous biopolymers, e.g., fibrous celluloses are the main components of hemp, wheat straw, rice straw, bagasse, etc., and are considered to be inexhaustible and renewable resources for the production of functional biocomposites.

Recently, considerable interest inspired by their biological origin has been directed to micro- or nanofibrous cellulose and its filled composites because of their low cost, biocompatibility, bioactivity, nontoxicity, biodegradability and oxygen barrier properties, which give them numerous potential applications, such as drug delivery, tissue engineering, food packaging, etc. Considerable research has been carried out regarding the extraction of cellulose nanofibrils (CNF) from different sources. For example, by a combination of chemical and mechanical treatments, Jonoobi et al. (2009) isolated nanofibrils from unbleached and bleached kenaf pulp. The obtained nanofibrils showed higher crystallinity and thermal stability compared to the raw kenaf. Among

reported studies, CNF-reinforced plastics have received ever-increasing interest, such as reinforced phenolic resin (Nakagaito and Yano 2004, 2008), acrylic resin (Yano et al. 2005; Nogi et al. 2006) and polylactic acid (Chakraborty et al. 2005) composites. Panaitescu et al. (2007) prepared α-cellulose nanofibrils from mechanochemical treated pulp for reinforced polypropylene composites. The composites exhibited higher tensile strength and elastic modulus than pure polypropylene. In comparison to cellulose nanocrystals or whisker reinforced (except for the cellulose nanowhiskers isolated from tunicate) composites, CNF-reinforced composites showed higher mechanical properties because of the higher aspect ratio of CNF (Cheng et al. 2009; Liu et al. 2010; Siqueira et al. 2009). Additionally, the flexibility of CNF could produce more flexible composites as compared with the stiff cellulose nanocrystals or whiskers.

Recently, incorporation of nanosized CNF into biodegradable polymer matrix has been explored as an important strategy for obtaining nanocomposites with environmentally friendly performance (Habibi et al. 2010; Eichhorn et al. 2010); for instance, polylactic acid nanocomposites reinforced with CNF also showed improved mechanical properties (Iwatake et al. 2008; Suryanegara et al. 2009; Jonoobi et al. 2010). Although extensive work has been done to prepare the commercial potential of cellulose nanofibril-filled biodegradable polymer materials (Eichhorn et al. 2010; Samir et al. 2004), poor mechanical behavior is still a key problem restricting their applications. Poly(vinyl alcohol) (PVA) is the largest and most popular synthetic water-soluble, semicrystalline, nontoxic, transparent and biocompatible as well as biodegradable polymer produced in the world. The degree of solubility, and the biodegradability as well as other physical properties can be controlled by varying the molecular weight and the degree of hydrolysis (saponification) of its mother polymer-polyvinyl acetate. PVA is used in a broad spectrum of applications in tissue scaffolding, filtration materials, membranes, optics, protective clothing, enzyme immobilization and drug release, etc. However, the low mechanical strength and integrity of PVA demand the use of reinforcing agents, for example, carbon nanotubes (Jeong et al. 2007; Wong et al. 2009), cellulose nanofibrils and chitin whiskers.

In this study, based on our former technology of joint mechanical treatment, paper pulp was also defibrillated into nanofibrils well dispersed in aqueous suspension. PVA/CNF nanocomposite films were prepared by the solution casting method from mixtures of PVA solution and CNF suspensions. Consequently, the chemical or crystalline structure, morphology, and thermal and mechanical properties of the nanocomposite films were also investigated. This study led to making a novel nanocomposite film based on a PVA solution and offered an eco-friendly, effective method of fabricating CNF-based biodegradable green materials with enhanced properties for high-end application.

Experimental section

Materials

The paper pulp was kindly provided by Domtar Corp. of Canada. PVA (AH-26) was purchased from Shanghai Sinopharm Chemical Reagent Co., Ltd., China.

Preparation of CNF

A certain amount of pulp was torn into small pieces and then poured into boiling water for several hours. The resulting pulp at a concentration of 1 wt% was beaten in a wet-grinding machine (Labor-Pilot 2000/4, IKA Works, Inc.) with a milling gap of about 0.1 mm at a flow speed of 10 l/h for 20 cycles. The pretreated pulp was then subjected to the high-pressure homogenizer (M-100P, Microfluidics Co., USA) under the constant pressure of 250 MPa for 20 cycles. The obtained suspended cellulose nanoparticles labeled as CNF were freeze-dried into powder for further characterization and blending experiments.

Preparation of CNF-reinforced PVA films

PVA was dissolved in distilled water at 90 °C under agitation for 1 h. After filtering out undissolved matter, we obtained a solution of PVA at a concentration of 10 wt%. The resulting PVA solution and CNF suspensions were mixed together under agitation to obtain blends with different compositions. After vacuum defoaming, the blend suspensions were cast into films at 25 °C. According to the weight ratio of CNF in the composites, i.e., 0.0, 1.0, 3.0, 5.0, 8.0, 10.0, 15.0, 20.0, 40.0 and 60.0 wt%, the nanocomposite films were coded as PVA, PVACNF1, PVACNF3, PVACNF5, PVACNF8, PVACNF10, PVACNF15, PVACNF20, PVACNF40 and PVACNF60, respectively.

Characterization

Transmission electron microscopy (TEM) observations were carried out on a JEOL JEM 2010 FEF (UHR) electron microscope with an accelerating voltage of 200 kV. One drop of diluted CNF suspension was spread on the copper grid coated with carbon support film and then coated with carbon for TEM observation. Scanning electron microscopy (SEM) was performed to investigate the morphology of the PVACNF composite films with an S-570 SEM (Hitachi, Japan) instrument. The tensile fractured surfaces of selected samples were mounted on SEM stands, coated with gold on an ion sputter coater and observed at 20 kV by SEM. FT-IR was recorded on a Thermo Nicolet Nexus 671 FT-IR using a KBr pellet method with a resolution of 4 cm^{-1}. X-ray diffraction diffractograms were recorded on a diffractometer (LabX XRD-6100, Shimadzu) in reflection mode in the angular range of 4°–60° (2θ) at a scanning rate of 0.5°/s. Differential scanning calorimetry (DSC) and thermogravimetric analysis (TGA) were performed on a SDT Q600 V20.9 from TA Instruments under helium flow (100 ml/min). The dry samples weighing between 3 and 10 mg were packed in aluminum pans, placed in the DSC cell and tested from ambient temperature to 600 °C at a heating rate of 10 °C/min under nitrogen atmosphere. Mechanical properties of the films were measured with a tensile testing machine (Instron Universal testing machine 5565) following ASTM standard D882. The initial distance between the grips was 25 mm, and the separation rate of the grips was kept constant at 4 mm/min. The stress–strain curve was recorded for each sample at 25 °C and relative humidity (RH) of 50 %, and the reported data in the manuscript were averaged over eight specimens. The percent optical transmittance (Tr) of the sheets with a thickness of about 0.4 mm was measured with a Perkin-Elmer ultraviolet–visible spectrometer (Lambda 3B model) in the wavelength range from 800 to 200 nm.

Results and discussion

Morphology of CNF

TEM micrographs of CNFs are shown in Fig. 1. CNFs exhibited widely distributed width ranging from 20 to 80 nm and length of more than a few microns. In fact, CNFs appearing like aggregated bundles consisted of thin wire-like microfibrils with diameters of a few nanometers. In this study, the associated large bundles, a number of branches of smaller bundles or partly individualized nanofibrils possessed a high aspect ratio of more than 50. A recent review dedicated to research into cellulose-based nanocomposites reported that an efficient reinforcement effect in composite materials can be guaranteed when nanofibrils with an aspect ratio around 50 are incorporated into a polymer matrix compared with conventional micro-sized fibrils (Gilberto et al. 2013).

Structure of the nanocomposites

The FT-IR spectra of CNF, PVA and composites are displayed in Fig. 2. An important absorption peak was verified at 1,143 cm^{-1}, which is associated with the C–C stretching mode of PVA and is generally related to the crystallinity of PVA (Tadokoro et al. 1956). The characteristic absorption bands of PVA occurring at 1,088, 919 and 838 cm^{-1} were attributed to the stretching of C–O, bending of –CH$_2$ and rocking of –CH, respectively. The absorption band at 1,058, 895 cm^{-1} in the spectra of CNF is attributed to the C–O stretching vibration and anomeric carbon of β-D-glucopyranosyl of cellulose, indicating the typical structure of cellulose (Huang et al. 2011), whereas the peak position of the C–O stretching vibration of cellulose and PVA shifted toward each other, which might contribute to the expected interaction of hydroxyl groups of PVA with the hydrophilic surfaces of the cellulose nanofibrils (Elizabeth et al. 2006).

Diffraction patterns of PVA, CNF and PVACNF characterized by XRD are shown in Fig. 3. A broad peak at 2θ = 19.4° observed from the profile of pure PVA film was attributed to the orthorhombic lattice structure of semi-crystalline PVA (Kurumova et al. 2000). There is a relative decrease in the intensity of the peak at 2θ = 19.4° with the increase of concentration of CNF; meanwhile, the diffraction peak of the 2θ angles at about 22.5° was assigned to the typical reflection planes (002), and the broad peak at around 16° was attributed (101) and (10$\bar{1}$) planes of cellulose I (Liu et al. 2010). Furthermore, the intensity of these
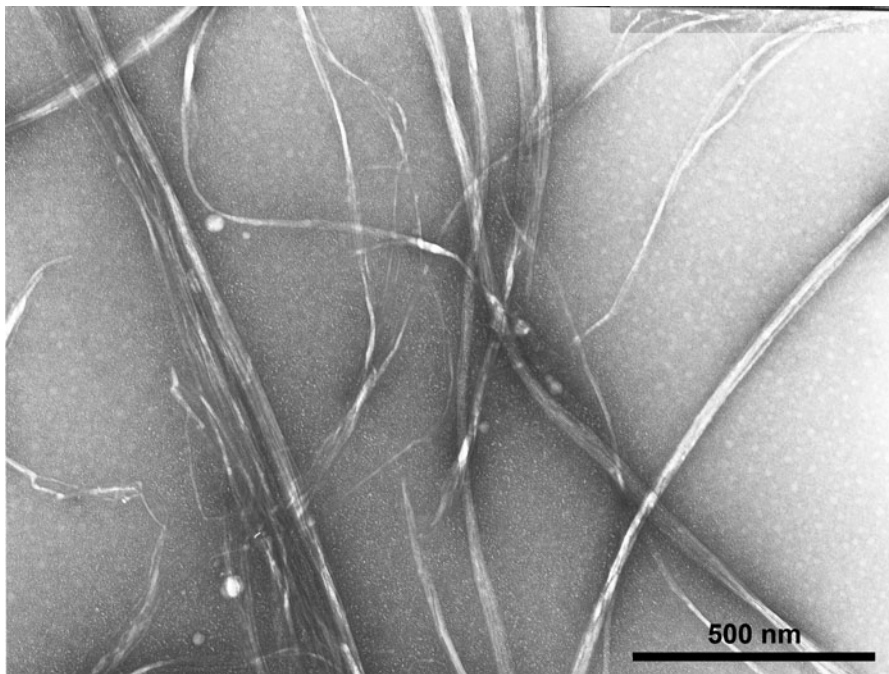
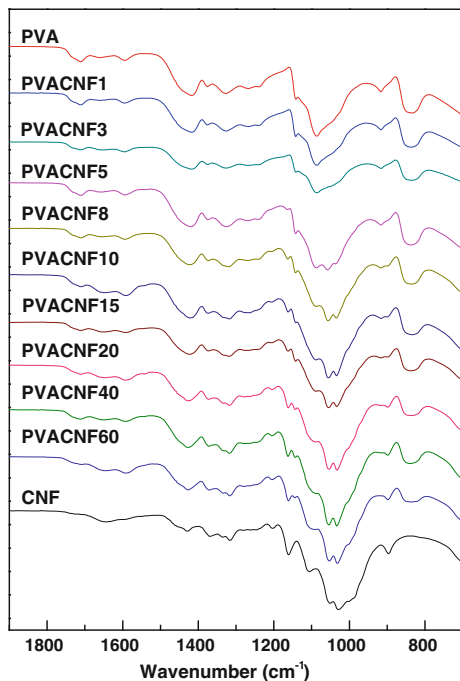**Fig. 1** TEM micrograph of cellulose nanofibers

Fig. 2 FT-IR spectra of pure PVA, CNF and PVACNF composites

two peaks increased with the increment of CNF in the nanocomposites. The degree of crystallinity (W) could be evaluated using the following relation:

$$W = 100 \ (S/S_o) \tag{1}$$

where S is the sum of the areas of all the crystallinity peaks and S_o is the total area under diffractogram (Prajapati and Gupta 2011). French (2013) also precisely described the crystallinity of small crystals by simulation with the Mercury program. In this work, we calculated the crystallinity using the program provided by LabX XRD-6100, and the degree of crystallinity of PVA, PVACNF3, PVACNF5, PVACNF10, PVACNF15, PVACNF20, PVACNF40, PVACNF60 and CNF was 28.2, 31.1, 33.4, 38.2, 42.5, 46.0, 58.7, 66.2 and 71.2 %, respectively. In fact, there was a linear relationship between the crystallinity and the content of CNF in the composites. CNF has a higher crystallinity than pure PVA; therefore, with the increment of the content of CNF, the crystallinity of the PVA/CNF composites increased accordingly.

Mechanical properties

The mechanical properties of the PVA and its composite films are listed in Table 1, and the typical stress–strain curves are shown in Fig. 4. Pure PVA film presented maximum stress of 29.7 MPa and elongation at break of 164.1 %, while the tensile
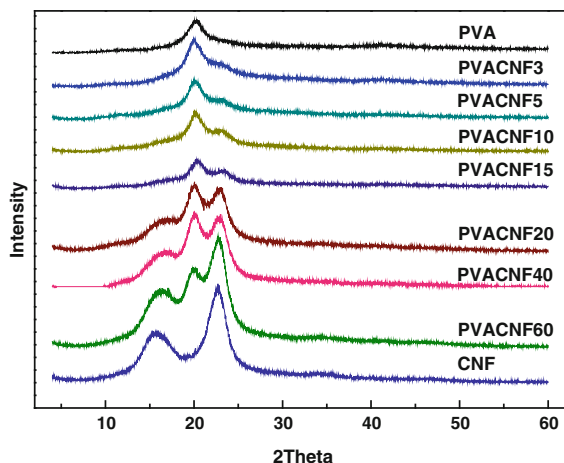
Fig. 3 X-ray diffraction patterns of PVA, CNF and PVACNF composite films. The degree of crystallinity of PVA, PVACNF3, PVACNF5, PVACNF10, PVACNF15, PVACNF20, PVACNF40, PVACNF60 and CNF was 28.2, 31.1, 33.4, 38.2, 42.5, 46.0, 58.7, 66.2 and 71.2 %, respectively

Table 1 Mechanical properties of the composite films

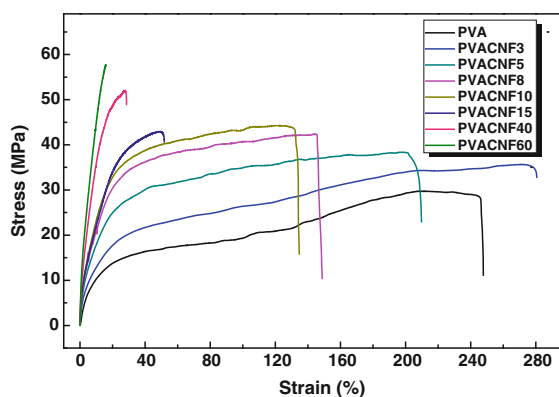| Samples	Tensile strain (%)	Tensile strength (MPa)	Young's modulus (MPa)
PVA	247.8 ± 30.0	29.7 ± 0.8	164 .1 ± 25.0
PVACNF3	280.7 ± 5.5	35.6 ± 0.7	228.1 ± 2.0
PVACNF5	255.5 ± 5.0	38.4 ± 2.6	378.2 ± 53.1
PVACNF8	148.8 ± 6.4	42.4 ± 3.3	442.2 ± 84.2
PVACNF10	134.8 ± 14.1	44.2 ± 0.9	476.6 ± 11.1
PVACNF15	51.8 ± 3.4	42.9 ± 6.8	509.2 ± 7.4
PVACNF40	28.5 ± 7.1	51.9 ± 2.3	876.4 ± 75.4
PVACNF60	19.1 ± 3.1	55.6 ± 2.1	1,022.3 ± 83.3

Fig. 4 Stress–strain curves of the films reinforced with 0, 3, 5, 8, 10, 15, 40 and 60 wt% CNF (based on the PVA weight)

stress, strain and modulus of PVA composite loading 3 % CNF were all improved about 20 %, respectively, with respect to the pure PVA film. The tensile stress and modulus of the composites kept on increasing with increasing content of CNF from 5 to 60 %, e.g., the tensile stress and Young's modulus of PVACNF60 were 57.7 and 1105.6 MPa, respectively, which were 1.9 and 6.2 times higher than pure PVA film. This indicates the nanocomposites exhibited much higher tensile strength and Young's modulus, and more rigid features with higher load-bearing capacity, indicating that CNF with high crystallinity can be used as a good reinforcement with the desired toughness to improve the mechanical strength of PVA-based films. However, as compared with pure PVA, films loading with 5–60 wt% CNF showed a trend of decreased elongation. That is to say, PVA behaves like an elastomer; PVACNF60 is really a rigid plastic with a high modulus of more than 1 GPa. In contrast to this, PVACNF3 possessed the highest elongation of all fabricated composites. This might be due to the optimized compatibility of CNF and PVA, which made PVACNF3 a highly toughened and flexible material. The enhancement of mechanical properties of PVACNF composites was suggested to have resulted from the good adhesion at the CNF/PVA matrix interface and the incorporation of stiff CNF with high crystallinity. (Lee et al. 2009; Roohani et al. 2008).

In order to better understand the mechanical properties of the PVACNF nanocomposites, SEM micrographs of the fractured cross-section are shown in Fig. 5. The fractured surface of pure PVA was rather flat and smooth with continuous flow, indicating that elastomer deformation of the matrix occurred with a specified load. In addition, the preferential tensile orientation was observed for pure PVA. This is why pure PVA exhibited a "drawing" at strains when the stress reached a plateau before failure, as shown in Fig. 4. In contrast, layered structures with uniformly dispersed cellulose sheets in PVA matrix were clearly revealed in the composites. A small amount (3 %) of incorporation of CNF would improve the ductility of the materials as evidenced by CNF sticking out of the fracture surface. On the fracture surfaces of high-loading CNF composite films, cellulose nanofibrils tended to align parallel to the film surface, resulting in the formation of an ultra-strong paper-like material

Fig. 5 SEM micrographs
of films **a** PVA;
b PVACNF3; **c** PVACNF5;
d PVACNF8;
e PVACNF10;
f PVACNF15;
g PVACNF20; **h** CNF
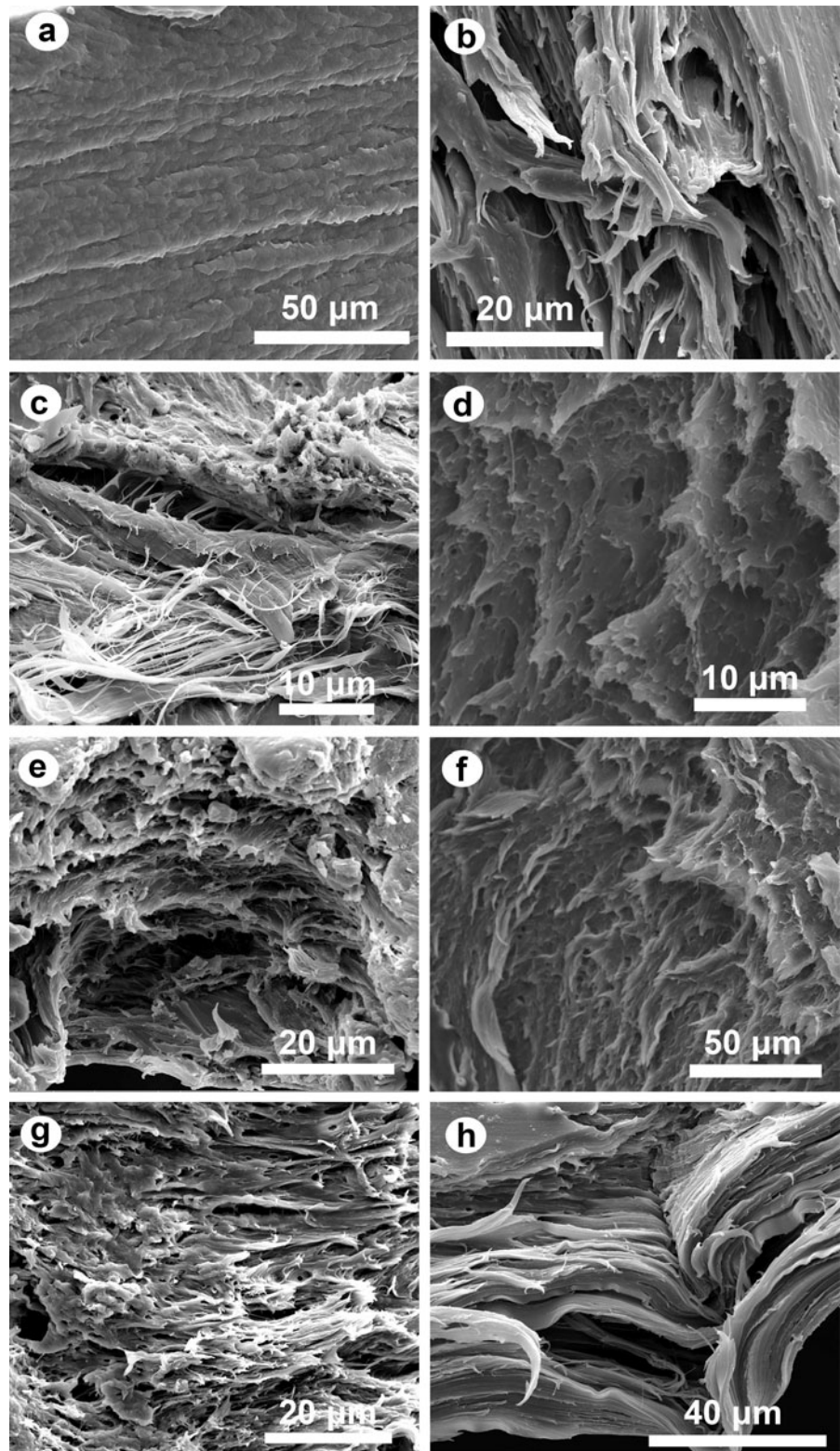
with layered structures. Therefore, the ductile fracture of the high-loading CNF composite exhibited in Fig. 4 also proved the rigid character of the CNF bundles surrounded by PVA matrix. In this continuous CNF network, PVA behaved like an adhesive to glue all the oriented nanofibrils together. With the decrease of PVA as an "adhesive," the cross-section exhibited brittle breaks. Without the connection of PVA, the pure CNF showed a morph of fault pictures. Therefore, CNF arranged in a layered structure was beneficial for improving the mechanical strength of the composites (Yang et al. 2010, 2011; Xu et al. 2009); simultaneously, PVA bound to fibrils was good for elevating the extension of the composites.

Thermal behaviors

DSC thermograms of PVA and PVACNF composites are presented in Fig. 6. The glass transition temperature (T_g) of PVA, PVACNF1, PVACNF3, PVACNF5, PVACNF8, PVACNF10, PVACNF15, PVACNF20, PVACNF40 and PVACNF60 were 77.4, 78.2, 79.1, 79.7, 80.1, 80.8, 81.7, 82.1, 82.8 and 83.2 °C, respectively. Obviously, the T_g of the nanocomposites was enhanced with the increase of CNF. Since T_g is related to the flexibility of polymeric segments, the result may be ascribed to the restriction of segmental motions of PVA chains. This behavior can be explained in that PVA chains were highly confined by cellulose nanofibrils because of the strong interactions, such as hydrogen bonding, between them. The expected interactions between these cellulose nanofibrils and PVA altered the supramolecular structure of the amorphous phase and decreased the mobility of the macromolecules at higher temperature. Therefore, the segmental motions of the PVA chains were greatly constricted and the chain mobility associated with glass transition slowed down, thus increasing the energy for glass transition to occur.

Figure 7 shows typical TGA and DTG curves of the composite films. All samples exhibited three distinct weight loss stages at 30–210 °C (5 wt% loss of weakly physic-sorbed water), 210–380 °C (decomposition of side chain of PVA) and 380–550 °C (decomposition of main chain of PVA). Major weight losses of about 75 wt% were observed in the range of 210–550 °C for all the samples, which corresponds to the structural decomposition of PVA and partly thermal degradation of CNF. The maximum
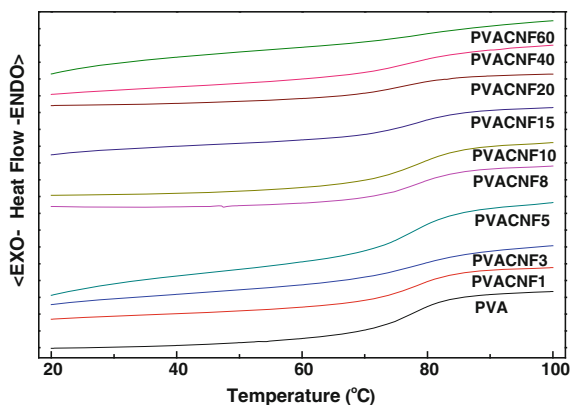

Fig. 6 DSC thermograms of composites reinforced with 0, 1, 3, 5, 8, 10, 15, 20, 40 and 60 wt% CNF. The T_g of PVA, PVACNF1, PVACNF3, PVACNF5, PVACNF8, PVACNF10, PVACNF15, PVACNF20, PVACNF40 and PVACNF60 was 77.4, 78.2, 79.1, 79.7, 80.1, 80.8, 81.7, 82.1, 82.8 and 83.2 °C, respectively
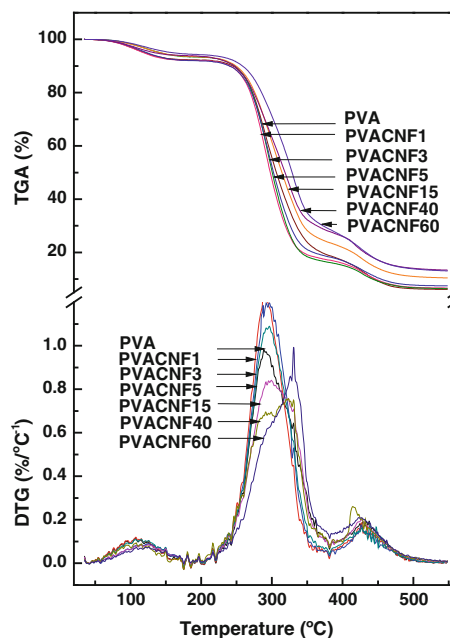

Fig. 7 TGA and DTG curves for the pure PVA and PVACNF composite films. Peak temperature (T_{max}) of PVA, PVACNF1, PVACNF3, PVACNF5, PVACNF15, PVACNF40 and PVACNF60 was 288, 291, 295, 296, 298, 321 and 331 °C, respectively)

decomposition rates related to T_{max} (the decomposition temperature corresponding to the maximum weight loss) revealed that the thermal decomposition behavior of the composites is similar to that of the pure

PVA. The maximum mass loss rates of the PVA/ cellulose nanofibril composites shifted to a higher temperature compared to that of pure PVA. However, this process was accompanied by an increase of T_{max} from 288 to 331 °C for PVA and PVACNF60, respectively, in its maximum mass loss rate upon addition of CNF. Over about 500 °C, TGA diagrams of all samples became flat, and mainly the inorganic residue remained. From the amounts of the residue at 550 °C, the residues of PVA and PVACNF60 were estimated to be approximately 6 and 13 wt%, respectively. Evidently, the thermal decomposition of PVACNF films shifted slightly toward high temperature, suggesting that the composite films had higher thermal stability mainly because of the presence of the crystal structure and thermal stability of CNF.

Optical transmissivity

It is well known that PVA is a kind of good optical material because of good optical transmissivity of its film, which can be evidenced from UV–visible curves of the PVA shown in Fig. 8. PVA composites with loading of 1, 3, 5, 10, 15, 20, 40 and 60 wt% CNF showed a reduction trend of the transparency, although these composites presented the transmittance of visible light higher than 40 %. Meanwhile, the composite film exhibited characteristic absorption of ultraviolet light at 200–275 nm, which is responsible for any charge transfer (Falcão and Azevêdo 2002). No red or blue shift of these bands indicated any charge transfer of chemical change in the composites during the addition of CNF. Therefore, composite film with an optimum amount of CNF will have high absorption of ultraviolet light and slight less transparency of visible light.
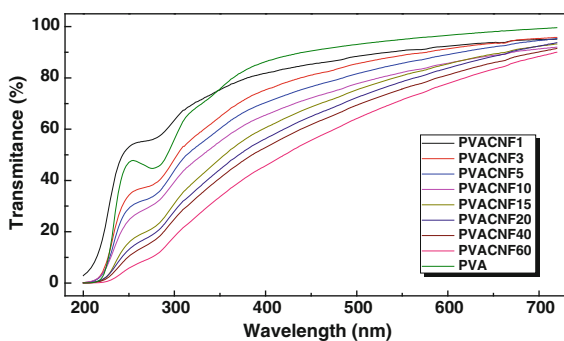

Fig. 8 UV–visible curves of the PVA and PVACNF composites with loading 1, 3, 5, 10, 15, 20, 40 and 60 wt% CNF

Conclusions

Cellulose nanofibril was successfully defibrillated by means of mechanical grinding and high pressure homogenization without any chemical treatments. When the CNF with a high aspect ratio and crystallinity was used to blend with PVA, both components showed good compatibility due to hydrogen bonding interaction. The well-dispersed CNF showed good reinforcement effects on the PVA matrix, e.g., the tensile stress and modulus were greatly enhanced. In the case of low-loading CNF (less than 5 wt%), the strains were even elevated, indicating good toughening effects. PVA behaved like an adhesive to bound stiff nanofibrils together and help to improve the elastic properties of the composites, which can be identified by SEM. The nanocomposite film also exhibited improved thermal stability and T_g compared with the pure PVA film. In addition, the nanocomposite films presented moderate transparency and good absorption of ultraviolet rays; they are promising materials for application in the optical and other functional engineering fields.

References

Chakraborty A, Sain M, Kortschot M (2005) Cellulose microfibrils: a novel method of preparation using high shear refining and cryocrushing. Holzforschung 59:102–107

Cheng QZ, Wang SQ, Rials TG (2009) Poly vinyl alcohol nanocomposites reinforced with cellulose fibrils isolated by high intensity ultrasonication. Compos Part A 40:218–224

Eichhorn SJ, Dufresne A, Aranguren M, Marcovich NE, Capadona JR, Rowan SJ, Weder C, Thielemans W, Roman M, Renneckar S, Gindl W, Veigel S, Keckes J, Yano H, Abe K, Nogi M, Nakagaito AN, Mangalam A, Simonsen J, Benight AS, Bismarck A, Berglund LA, Peijs T (2010) Review: current international research into cellulose nanofibres and nanocomposites. J Mater Sci 45:1–33

Elizabeth FR, Fábia SC, Andrey PL, Romulo CL, Luiz GH, Wander LV, Zelia IPL, Herman SM (2006) Synthesis and characterization of poly (vinyl alcohol) hydrogels and hybrids for rMPB70 protein adsorption. Mater Res 9(2):185–191

Falcão EHL, Azevêdo WM (2002) Polyaniline–poly(vinyl alcohol) composite as an optical recording material. Synth Metals 128:149–154

French AD (2013) Idealized powder diffraction patterns for cellulose polymorphs. Cellulose. doi:10.1007/s10570-013-0030-4

Gilberto S, Julien B, Nadège F, Sabrina B, Stéphane M, Alain D (2013) Thermal and mechanical properties of bio-nanocomposites reinforced by *Luffa cylindrica* cellulose nanocrystals. Carbohydr Polym 91(2):711–717

Habibi Y, Lucia LA, Rojas OJ (2010) Cellulose nanocrystals: chemistry, self-assembly, and applications. Chem Rev 110:3479–3500

Huang B, Tang LR, Dai DS, Ou W, Li T, Chen XR (2011) Biomaterials science and engineering. Plenum Press, Croatia, pp 139–153

Iwatake A, Nogi M, Yano H (2008) Cellulose nanofiber-reinforced polylactic acid. Compos Sci Technol 68:2103–2106

Jeong BH, Hoek EMV, Yan YS, Subramani A, Huang XF, Hurwitz G, Ghosh AK, Jawor A (2007) Interfacial polymerization of thin film nanocomposites: a new concept for reverse osmosis membranes. J Membr Sci 294(1–2):1–7

Jonoobi M, Harun J, Shakeri A, Misra M, Oksman K (2009) Chemical composition, crystallinity, and thermal degradation of bleached and unbleached kenaf bast (*Hibiscus cannabinus*) pulp and nanofibers. BioResources 4(2): 626–639

Jonoobi M, Harun J, Mathew AP, Oksman K (2010) Mechanical properties of cellulose nanofiber (CNF) reinforced polylactic acid (PLA) prepared by twin screw extrusion. Compos Sci Technol 70:1742–1747

Kurumova M, Lopez D, Benevente R, Mijangos C, Perena JM (2000) Effect of crosslinking on the mechanical and thermal properties of poly(vinyl alcohol). Polymer 41: 9265–9272

Lee SY, Mohan DJ, Kang IA, Doh GH, Lee S, Han SO (2009) Nanocellulose reinforced PVA composite films: effects of acid treatment and filler loading. Fiber Polym 10(1):77–82

Liu D, Zhong T, Chang PR, Li K, Wu Q (2010) Starch composites reinforced by bamboo cellulosic crystals. Bioresour Technol 101(7):2529–2536

Nakagaito AN, Yano H (2004) The effect of morphological changes from pulp fiber towards nano-scale fibrillated cellulose on the mechanical properties of high strength plant fiber based composites. Appl Phys A 78(4):547–552

Nakagaito AN, Yano H (2008) The effect of fiber content on the mechanical and thermal expansion properties of biocomposites based on microfibrillated cellulose. Cellulose 15(4):555–559

Nogi M, Shinsuke I, Kentaro A, Keishin H, Nakagaito AN, Hiroyuki Y (2006) Fiber-content dependency of the optical transparency and thermal expansion of bacterial nanofiber reinforced composites. Appl Phys Lett 88(13): 133124–133127

Panaitescu DM, Nechita P, Iovu H, Iorga MD, Ghiurea M, Serban D (2007) Compozite din polipropilena si microfibrile celulozice obtinute prin tratamente mecano-chimice. Mater Plast 44(3):195–198

Prajapati GK, Gupta PN (2011) Comparative study of the electrical and dielectric properties of PVA–PEG–Al_2O_3–MI (M = Na, K, Ag) complex polymer electrolytes. Physica B 406(15–16):3108–3113

Roohani M, Habibi Y, Belgacem NM, Ebrahim G, Karimi AN, Dufresne A (2008) Cellulose whiskers reinforced polyvinyl alcohol copolymers nanocomposites. Eur Polym J 44(8):2489–2498

Samir MASA, Alloin F, Paillet M, Dufresne A (2004) Tangling effect in fibrillated cellulose reinforced nanocomposites. Macromolecules 37:4313–4316

Schmidt G, Malwitz MM (2003) Properties of polymer–nanoparticle composites. Curr Opin Colloid Interface Sci 8:103–108

Siqueira G, Bras J, Dufresne A (2009) Cellulose whiskers versus microfibrils: influence of the nature of the nanoparticle and its surface functionalization on the thermal and mechanical properties of nanocomposites. Biomacromolecules 10(2): 425–432

Suryanegara L, Nakagaito AN, Yano H (2009) The effect of crystallization of PLA on the thermal and mechanical properties of microfibrillated cellulose-reinforced PLA composites. Compos Sci Technol 69(7–8):1187–1192

Tadokoro H, Seki S, Nitta I (1956) Some information on the infrared absorption spectrum of polyvinyl alcohol from deuteration and pleochroism. J Polym Sci 22:563–566

Wong KKH, Hutter JL, Zinke-Allmang M, Wan W (2009) Physical properties of ion beam treated electrospun poly(vinyl alcohol) nanofibers. Eur Polym J 45(5):1349–1358

Xu Y, Hong W, Bai H, Li C, Shi G (2009) Strong and ductile poly(vinyl alcohol)/graphene oxide composite films with a layered structure. Carbon 47(15):3538–3543

Yang X, Li L, Shang S, Tao XM (2010) Synthesis and characterization of layer-aligned poly(vinyl alcohol)/graphene nanocomposites. Polymer 51:3431–3435

Yang X, Shang S, Li L (2011) Layer-structured poly(vinyl alcohol)/graphene oxide nanocomposites with improved thermal and mechanical properties. J Appl Polym Sci 120:1355–1360

Yano H, Sugiyama J, Nakagaito AN, Nogi M, Matsuura T, Hikita M, Handa K (2005) Optically transparent composites reinforced with networks of bacterial nanofibers. Adv Mater 17(2):153–155